Quaternary International 310 (2013) 47–61

Contents lists available at SciVerse ScienceDirect

Quaternary International

journal homepage: www.elsevier.com/locate/quaint

Forcing of hydroclimatic variability in the northwestern Great Plains since AD 1406

Suzan L. Lapp, Jeannine-Marie St. Jacques*, David J. Sauchyn, Jessica R. Vanstone

Prairie Adaptation Research Collaborative (P.A.R.C.), Room 120, 2 Research Drive, University of Regina, Regina, Saskatchewan, Canada S4S 7H9

ARTICLE INFO

Article history:
Available online 18 September 2012

ABSTRACT

The 20th century hydroclimatology of northwestern North America has been linked to naturally recurring large-scale climate patterns such as the Pacific Decadal Oscillation (PDO) and the El Niño-Southern Oscillation (ENSO). Few observed hydroclimatic records from this region exceed in length the ~60-year periodicity of the lower frequency climate oscillations; however, tree-ring proxy data from semi-arid western North America document natural hydroclimate variation over centennial to millennial scales. We reconstructed the summer Palmer Drought Severity Index (PDSI) over the western Canadian Prairies, providing a record of drought for the past 600 years. This long reconstruction was examined for information about the severity, intensity, and duration of positive (wet) and negative (dry) summer moisture anomalies during the different phases of the PDO and the ENSO, as reconstructed by other researchers from independent proxy datasets. As well, by comparing our PDSI reconstruction to other researchers' independent regional summer temperature reconstruction, we were able to identify warm versus cold droughts, and warm versus cold wet periods. The reconstruction was also compared to 500 hPa geopotential heights. These results suggest that summer moisture conditions are associated with the North Pacific Ocean and tropical Pacific Ocean variability. Summer droughts generally have occurred during the positive PDO phase; however, ENSO conditions have varied between El Niño and La Niña. The most severe droughts, such as those of AD 1858–1872 and AD 1930–1941, were commonly associated with higher summer temperatures, the positive phase of the PDO, and increased ENSO variability.

1. Introduction

Numerous studies have shown significant associations between the large-scale atmosphere–ocean teleconnections, specifically the Pacific Decadal Oscillation (PDO) and the El Niño-Southern Oscillation (ENSO), and variations in the 20th century northwestern North American hydroclimate, including that of the Northern Great Plains (Mantua and Hare, 2002; MacDonald and Case, 2005; Bonsal et al., 2006; Nyenzi and Lefale, 2006; Ault and St. George, 2010; St. Jacques et al., 2010). These hydroclimatic fluctuations at interannual to multi-decadal timescales have been associated with severe droughts and floods causing extreme damage and economic hardship (Wheaton et al., 2005; Garnett et al., 2006; Cook et al., 2007; Gan et al., 2007; Bonsal et al., 2011). Single-year extremes of drought and excess moisture are damaging, but are not necessarily good indicators of cumulative environmental and socioeconomic impacts. The critical indicator is duration, since recovery from the cumulative damage of a multi-year event is more challenging than from a single extreme year (Wheaton et al., 2005; Cook et al., 2007; Marchildon et al., 2008). The future climatology of extreme drought and excessive moisture in the northern Prairies are of substantial relevance, given drought's historical impacts, and projections of increased frequency and climate extremes associated with human induced climate change (Kharin et al., 2007; Bonsal et al., 2011).

The associations between the PDO and ENSO and the climate of northwestern North America are well established for the instrumental period. The PDO is a re-occurring sea surface temperature (SST) anomaly pattern that describes a large amount of extra-tropical North Pacific Ocean variability (Mantua et al., 1997; Zhang et al., 1997; Mantua and Hare, 2002). The warm, positive PDO phase has anomalously warm SSTs off the west coast of North America and a deepened Aleutian Low, resulting in decreased winter precipitation throughout northwestern North America; opposite conditions exist for the cold, negative phase of the PDO (Mantua et al., 1997; St. Jacques et al., 2010; Bonsal et al., 2011). The strength of the Aleutian Low pressure system covaries with the North Pacific SST anomalies (IPCC4, 2007) by

* Corresponding author.
E-mail address: stjacqje@uregina.ca (J.-M. St. Jacques).

1040-6182/$ – see front matter © 2012 Elsevier Ltd and INQUA. All rights reserved.
http://dx.doi.org/10.1016/j.quaint.2012.09.011

shifting the storm track and impacting the downstream climate (Trenberth and Hurrell, 1994). A deepened Aleutian Low shifts the storm track to the north and a weakened Aleutian Low shifts it to the south. The interaction between the pentadecadal (50–70 years) and the bidecadal (15–25 years) temporal variations of the PDO modulate the winter and spring variability of the Aleutian Low, with the pentadecadal variability controlling the basin regime timescale shifts and the bidecadal variability controlling the rate of transition between the regimes (Minobe, 1999). A warm El Niño occurrence of ENSO typically has the same association with winter climate in northwestern North America as the positive phase of the PDO; a similar relationship is found between a cold La Niña and the negative phase of the PDO (Cayan et al., 1999; St. Jacques et al., 2010; Bonsal et al., 2011). These ENSO events can be further intensified by variations of the PDO; typically there are more occurrences of El Niño (La Niña) during the positive (negative) phase of the PDO (Kiem et al., 2003; Bonsal and Shabbar, 2011).

The relatively short instrumental climate record (~100 years) captures only approximately two full cycles of the low-frequency PDO, and therefore is unable to provide a robust assessment of the variability at the lower frequency oscillations (IPCC4, 2007). Tree-ring proxy data from semi-arid, western North America record natural hydroclimate variation over centuries to millennia (Biondi et al., 2001; Gedalof et al., 2002; MacDonald and Case, 2005; Axelson et al., 2009; Sauchyn et al., 2011). Moisture sensitive tree-rings capture the inter-annual to multi-decadal variability in summer/annual moisture and thus the periodicity in known large-scale drivers of climatic variability; and the frequency, severity, and duration of periods of sustained low and high moisture conditions (Woodhouse, 1997; Gedalof and Smith, 2001; Hughes, 2002). At dry sites, tree growth is limited by the available soil moisture, enabling the reconstruction of hydroclimatic variables such as precipitation, streamflow, forest fire frequency and area burned, and drought (Sauchyn and Skinner, 2001; Case and MacDonald, 2003; Sauchyn et al., 2003; Watson and Luckman, 2004, 2005a, 2005b; Girardin et al., 2006; Cook et al., 2007; Girardin and Sauchyn, 2008; Axelson et al., 2009; St. George et al., 2009). These long tree-ring records potentially provide more insight than that currently available in the instrumental record.

In this study, we examine the hydroclimatic variability (droughts, and wet periods or pluvials) over the past 600 years in the Canadian Prairies (Fig. 1), by reconstructing the summer Palmer Drought Severity Index (PDSI) using a network of moisture-sensitive tree-ring chronologies. Tree-rings in this northern Prairie region are best for reconstructing spring/summer soil moisture conditions (St. George et al., 2009; St. George et al., 2010). Because recurrent drought excludes trees from the northern Great Plains, the tree-ring record is mostly from sites on the forested margins of this region and a few island forests. We focused on the western margin of the Canadian Prairies where the tree-ring chronologies have the greatest length, approaching 1000 years (Sauchyn et al., 2011); the signal of SST forcing is most evident (St. Jacques et al., 2010); and the water supply for the majority of the population is generated. Here, antecedent winter precipitation has an important effect on growing season soil moisture. This prompts our hypothesis that decreased winter precipitation (*i.e.*, snowpack) has been an important precursor for periods of sustained drought in the recent past (and conversely for increased snowpack and sustained pluvials). Winter snowpack is strongly influenced by climate oscillations such as the PDO and ENSO. To examine the relationship between summer moisture anomalies and the winter

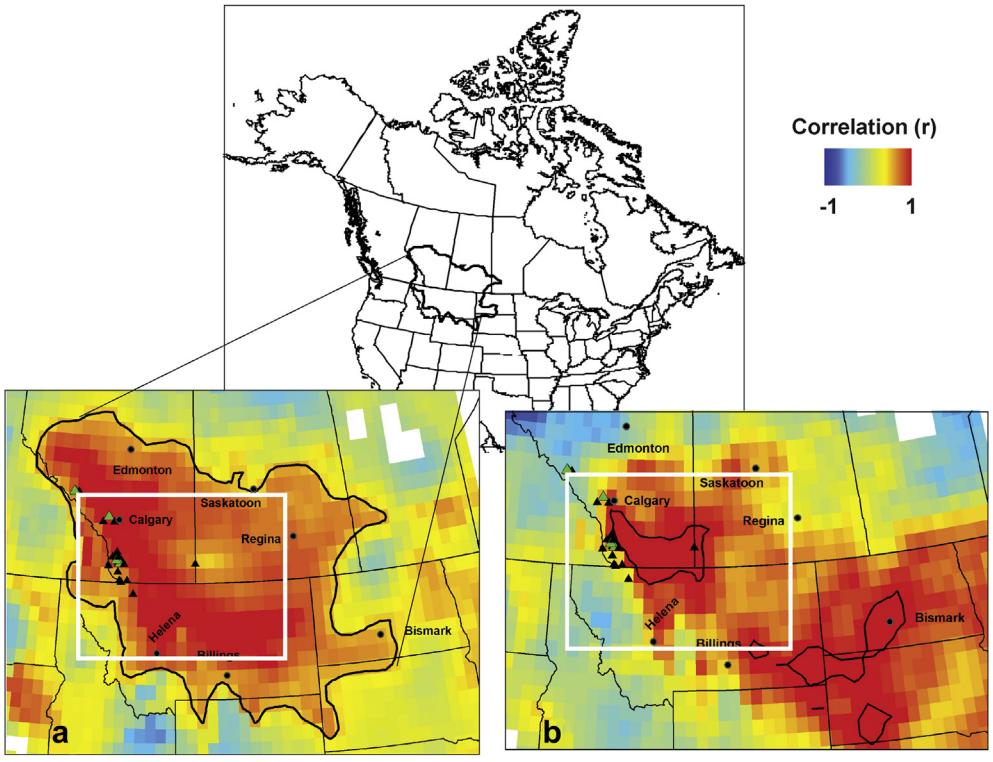

Fig. 1. Correlation maps between the instrumental summer Palmer Drought Severity Index (JJA PDSI) and (a) $PC1_{final}$ and (b) $PC2_{final}$, for AD 1901–2004 on the northwestern Great Plains. The white box outlines the initial study region (46–52°N and 105–116°W). The thick black line identifies positive correlation (Pearson's *r*) at the 99% significance level, adjusted for autocorrelation according to Dawdy and Matalas (1964). The green triangles represent the five longest tree-ring chronologies used to construct $PC1_{final}$ and $PC2_{final}$, and the black triangles represent the remaining 23 chronologies used for the common period principal component analysis. (For interpretation of the references to colour in this figure legend, the reader is referred to the web version of this article.)

Pacific Ocean teleconnection patterns, we compared our summer drought record to other researchers' PDO and ENSO reconstructions (*i.e.*, MacDonald and Case, 2005; Verdon and Franks, 2006; Cook et al., 2008). Based on the instrumental record, we hypothesized that sustained drought is more likely to occur during the positive PDO phase, and conversely that sustained pluvials are more likely to occur during the negative PDO phase. We also conjectured that more El Niño (La Niña) events would occur during a sustained drought (pluvial) than La Niña (El Niño) events or neutral states. Our overall goal was to explore possible forcing mechanisms for periods of sustained hydroclimate extremes. By comparing our moisture reconstruction to an independent mean summer temperature reconstruction (Luckman and Wilson, 2005), we also identified warm or cold droughts, and warm or cold pluvials.

2. Data and methods

2.1. Study area

Despite their relatively small area, the eastern slopes of the Rocky Mountains straddling the United States–Canadian border serve as a disproportionately large source of surface water supplies for the northern Prairies. They contain the headwaters of the Saskatchewan and Missouri Rivers, supplying the Saskatchewan River with 60% and the Missouri River with 73% of its annual flows (Pomeroy et al., 2005). On the eastern slopes, in the fall and winter, water is stored as snow and lake ice; and in the early spring, surface water supplies are derived from rapid initial snowmelt. Winter snowpack accumulation and spring melt are strongly affected by the winter climate oscillations and their winter teleconnections (Mantua et al., 1997; Shabbar et al., 1997; Gershunov and Barnett, 1998). Importantly for montane tree growth, continuing snowmelt water during the late spring and early summer replenishes soil moisture, whose stores are further augmented by warm season rainfall.

Over the eastern slopes of the Rockies and the Canadian Prairies, nearly half of the annual precipitation falls during the May–September period (Environment Canada, 2012; http://www.climate.weatheroffice.gc.ca/climate_normals/index_e.html). However, it is largely the other half of the annual precipitation that forms winter snowpack that recharges surface water and groundwater, not summer rainfall (Hamlet et al., 2007; Pomeroy et al., 2007; Pham et al., 2009).

2.2. Palmer Drought Severity Index

The Palmer Drought Severity Index (PDSI) is an index of meteorological drought widely used in North America. It is calculated using monthly temperature and precipitation data and the soil available water content (AWC) to express the cumulative departure of moisture supply (Palmer, 1965; Alley, 1984; Keyantash and Dracup, 2002). It is a standardized index that allows comparisons between different geographical locations and months. This index is preferred to drought indices based solely on precipitation, as it has considerable month-to-month persistence and better represents the basic terms of water balance, including evapotranspiration, soil recharge, runoff, and surface moisture loss. The intensity during the current month is dependent on the current weather patterns plus the antecedent conditions of previous months. The PDSI is derived by including one third of the current month's precipitation deficit or surplus, and almost nine-tenths of the previous month's value (Guttmann, 1998). For this reason, the PDSI is effective in capturing the cumulative effect of long-term drought or pluvial events. The index typically varies between −4.0 and 4.0, with values below −0.49 but greater than −1.0 (above 0.49 but less than 1.0) considered an "incipient dry spell" ("incipient wet spell"); and −1.0 (1.0) is the threshold value of an actual drought (pluvial) event (Table 1). Gridded (0.5°) summer June–July–August (JJA) PDSI time series for the northern Great Plains were calculated for the AD 1901–2004 period using the observed monthly baseline historical gridded (0.5°) precipitation and temperature climate data generated by the Canadian Forest Service (McKenney et al., 2006). Also used was gridded (0.5°) global AWC (in millimetres (mm) of water per one metre soil depth) from the Oak Ridge National Laboratory Distributed Active Archive Center (http://daac.ornl.gov) (Batjes, 2000).

Table 1
The Palmer Drought Severity Index (PDSI) of moisture classifications.

Classification	PDSI
Extreme drought	≤−4.0
Severe drought	>−4.0 to −3.0
Moderate drought	>−3.0 to −2.0
Mild drought	>−2.0 to −1.0
Incipient dry spell	>−1.0 to −0.5
Near normal	>−0.5 to <0.5
Incipient wet spell	0.5 to <1.0
Mildly wet	1.0 to <2.0
Moderately wet	2.0 to <3.0
Severely wet	3.0 to <4.0
Extremely wet	≥4.0

2.3. Tree-ring data

Researchers at the University of Regina Tree-Ring Laboratory have established a network of tree-ring chronologies that extends across the montane forest of the northern Rocky Mountains, and the island forests of the northern Great Plains (*i.e.*, Alberta, Saskatchewan and Montana; Fig. 1). We used chronologies located along the eastern slopes of the southern Canadian Rocky Mountains, which are the longest in our collection. The principle of site selection is important when developing a sensitive ring-width series (Stokes and Smiley, 1968; Speer, 2010) and the sampled trees are growing on the edge of their ecological niche on dry sites (*i.e.*, south- and west-facing slopes, sandy soils, and ridge crests). There is a strong correlation between these moisture-sensitive tree-ring width chronologies and the summer PDSI throughout the entire Canadian Prairie Region (St. George et al., 2009). Montane tree-ring variability is connected to winter climate oscillation variability by the late spring/early summer soil moisture recharge which is dependent upon winter snowpack accumulation and which sets up antecedent conditions for warm season growth.

In total, 28 site chronologies were significantly correlated ($p \leq 0.05$) with an instrumental JJA PDSI regional average computed over an initial study region (46–52°N and 105–116°W) (Fig. 1 and Appendix A Table A1). The individual tree-ring chronologies from each site were detrended using a 100-year cubic spine (50% cutoff) to maintain low frequency variability using the program ARSTAN (Cook, 1985; St. George et al., 2009). Both standard and residual tree-ring chronologies were examined. However, the highest correlations with PDSI data were found using the standard chronologies, which are used henceforth. The standardized ring-width series of various lengths were averaged using the arithmetic mean for each site, forming the site chronology. Subsample signal strength (SSS) was computed as a function of mean inter-tree correlation and sample size (Briffa and Jones, 1990). A SSS equal to or greater than 0.85 was used as the threshold for truncating the site chronology at a sample depth for a reliable chronology (Cook and Kairiukstis, 1990). The site chronologies ranged in length from 116 to 990 years.

Repeated Principal Component Analysis (PCA) was used to produce the longest possible reconstruction from the least number of chronologies, yet maintaining the same key information as the initial 28 site chronologies. First, PCA of the 28 standard site chronologies over a common period of AD 1926–2004 was performed using the covariance matrix, to yield an orthogonal set of new variables (Meko et al., 2007; St. George et al., 2009). Any chronologies that terminated prior to 2004 were extended using the mean value from the remaining chronologies (Kim and North, 1993). Next, we removed the shortest chronology, repeated the PCA on the remaining chronologies, and compared this PC1 from the reduced set to the first PC1 over the common period. This procedure was repeated until PC1 no longer shared the same signal as the common period PC1 (*i.e.*, Pearson correlation coefficient $r < 0.9$). Throughout the rest of this manuscript, $PC1_{final}$ and $PC2_{final}$ will refer to those from the penultimate of the iterated PCAs (*i.e.*, $r \geq 0.9$).

The $PC1_{final}$ study region was defined by selecting the instrumental PDSI gridcells whose JJA time series were highly significantly ($p \leq 0.01$) correlated with $PC1_{final}$ restricted to AD 1901–2004. A regional average, PC1 JJA PDSI, was then calculated using the data from these cells. Linear regression was applied to reconstruct PC1 JJA PDSI prior to the instrumental period using $PC1_{final}$ as the predictor.

Similarly, the $PC2_{final}$ study region, was defined by selecting the instrumental PDSI gridcells whose JJA time series were highly significantly ($p \leq 0.01$) correlated with $PC2_{final}$ restricted to AD 1901–2004. A regional average, PC2 JJA PDSI, was then calculated using the data from the cells comprising the $PC2_{final}$ study region. Again, linear regression was applied to reconstruct PC2 JJA PDSI prior to the instrumental period using $PC2_{final}$ as the predictor.

In order to verify that the expected climate signals were present, we screened the recent portions of $PC1_{final}$ and $PC2_{final}$ with instrumental data. First, $PC1_{final}$ was compared to instrumental mean previous December–current February precipitation and mean June–August precipitation averaged from the $PC1_{final}$ study region, using correlation analysis and data from McKenney et al. (2006) for AD 1901–2004. For comparison, the mean instrumental June–August PDSI from the $PC1_{final}$ study region was compared to instrumental mean December–February precipitation and mean June–August precipitation, again using correlation analysis for AD 1901–2004. Using composite analysis based upon a permutation two-sample *t*-test (10,000 iterations), we screened $PC1_{final}$ and $PC2_{final}$ for a PDO signal. We stratified the years AD 1901–2004 according to the low-frequency PDO phases of Minobe (1997, 1999); negative PDO: AD 1901–1924 and AD 1947–1976, and positive PDO: AD 1925–1946 and AD 1977–2004. Similarly using composite analysis based upon a permutation two-sample *t*-test (10,000 iterations), we screened $PC1_{final}$ and $PC2_{final}$ for an ENSO signal. We stratified the years AD 1872–2004 according to when the instrumental mean previous December–March Nino 3.4 index (Trenberth and Stepaniak, 2001) (http://www.cgd.ucar.edu/cas/catalog/climind/TNI_N34/index.html) exceeded 0.5 for El Niño and was less than −0.5 for La Niña.

2.4. Runs analysis to define drought and pluvial episodes

Typically the interpretation of tree-ring reconstructions of hydroclimate have focused on drought signals because these are stronger than records of pluvial events, and since water shortages are a major climate hazard. However, extreme pluvial episodes also have socio-economic and environmental consequences, and therefore are characterized in this study as well, even though extreme pluvial episodes are less well recorded. We used runs analysis (Dracup et al., 1980; Meko et al., 1995; Biondi et al., 2005) to categorize multi-year drought/pluvial episodes according to their duration, severity and intensity. Duration is the number of consecutive years (n) (Biondi et al., 2005) the PDSI remained below (above) a certain threshold value (X_o). The severity of the drought (pluvial) is the run-sum (sum of the deficits below (above) the X_o over the n years), and intensity is the average deviation from X_o (severity/duration). This analysis allowed us to rank episodes and identify the underlying persistent climate modes associated with extreme hydroclimatic events (Biondi et al., 2005). A PDSI of −0.49 (0.49) was chosen as the drought (pluvial) threshold value. Drought tends to be more prolonged than periods of excess water (Bonsal et al., 2011); therefore, drought (pluvial) events were considered extreme if they persisted for five (three) years or longer. If a drought of five years or longer included one or more non-successive year(s) with a PDSI greater than −0.49 but less than 0, then these were still considered drought years and were included in the total run-sum (severity) calculation. This same method was applied to pluvial episodes exceeding the three year baseline.

2.5. Additional proxy climate data

Because the PDO has such a strong effect on northwest North American climatology, we compared reconstructed PDO positive and negative phases to the drought and pluvial episodes defined by our summer PDSI reconstruction (PC1 JJA PDSI). There are numerous PDO reconstructions using tree-ring chronologies from the Pacific Northwest and subtropical North America (*e.g.*, Biondi et al., 2001; D'Arrigo et al., 2001; Gedalof and Smith, 2001; MacDonald and Case, 2005; D'Arrigo and Wilson, 2006; Verdon and Franks, 2006). Our analysis used the MacDonald and Case (2005) annual (January–December) PDO reconstruction (spanning AD 993–1996), with the Verdon and Franks (2006) composite reconstruction providing additional verification because of the many discrepancies among PDO reconstructions. The Verdon and Franks (2006) Composite PDO Index is derived from various PDO proxies and spans AD 1662–1998. Multi-decadal step changes in this Composite PDO index signify a switch from a predominately positive to a predominately negative phase period or vice-versa.

We also compared reconstructed ENSO events to the drought and pluvial episodes defined by our summer PDSI reconstruction (PC1 JJA PDSI). Again, numerous ENSO reconstructions have also been derived from proxy indicators influenced by ENSO (*e.g.*, Cook, 2000; Mann et al., 2000; Cook et al., 2008; McGregor et al., 2010). We used the longest (AD 1300–2006) and most recent Cook et al. (2008) December–February Niño 3.4 index reconstruction (5°S–5°N, 120°W–170°W), obtained from the World Data Center for Paleoclimatology (http://www.ncdc.noaa.gov/paleo/recons.html).

The PDO phases and ENSO events and variability were characterised for each drought and pluvial episode in our PDSI reconstruction. The MacDonald and Case PDO and the Composite PDO indices were used to identify the dominant PDO phase for their period of record (the rare disagreements between the two were flagged). Using the MacDonald and Case PDO reconstruction, the PDO index for each year of each drought or pluvial episode was summed; if the sum was positive (negative), the drought or pluvial was considered to have occurred in the positive (negative) PDO phase. The Composite PDO index consists of a time series of low frequency positive and negative PDO phases. In this case, it was simply noted whether each sustained drought and pluvial episode occurred during a positive PDO phase, a negative PDO phase or straddled a transition between the two phases. The type of ENSO occurrence was characterized for the

preceding year and each year of the drought or pluvial. In the Cook et al. (2008), El Niño events were defined by a Niño 3.4 index $\geq$ 0.4 and La Niña events by a Niño 3.4 index $\leq$ −0.4; otherwise a neutral event occurred. To assess ENSO variability, the variance of the Cook et al. (2008) index was calculated using a sliding 17-year window (value assigned to centre year of window). If the mean variance for the drought or pluvial episode was greater than the mean variance for AD 1300–2006 ($\delta^2 = 0.6$), the ENSO variance for the episode was considered to be high, otherwise it was considered to be low.

To explore the stability of the link between climate forcing and tree-ring response through time, 31-year running correlations were calculated between $PC1_{final}$ and $PC2_{final}$ and the reconstructed MacDonald and Case PDO and Cook et al. Niño 3.4 indices over AD 1406–1996 and AD 1406–2006, respectively. The instrumental January–December PDO index (Mantua et al., 1997) was used to extend the running correlations to 2004. All correlation values were adjusted for autocorrelation using Dawdy and Matalas (1964).

In order to compare sustained warm and cool periods in relation to drought and pluvial episodes defined by our summer PDSI reconstruction, we used Luckman and Wilson (2005) mean summer (May–August) temperature reconstruction for the south/central Canadian Rockies for AD 950–1994. They also identified the most extreme warm and cool, non-overlapping, 20-year intervals as calculated from the mean summer temperature reconstruction relative to the AD 1900–1980 period. It is the longest proxy temperature record from the Canadian Rockies, based upon multiple sites and providing a regional representation.

2.6. Spectral analysis and synoptic dynamics methods

Multi-taper method (MTM) spectral analysis (Thomson, 1982; Ghil et al., 2002) and Morlet Wavelet Analysis (Grinsted et al., 2004) were applied to the final principal components to identify dominant modes of variability. In the SSA-MTM Toolkit for MTM Spectral Analysis (http://www.atmos.ucla.edu/tcd/ssa/), we used adaptively weighted spectra with a red noise background (three tapers) (Mann and Lees, 1996). The wavelets were analyzed with MATLAB® (http://www.pol.ac.uk/home/research/waveletcoherence/). We were interested in the detection of variability at periodicities characteristic of the PDO (~20 and ~60 years) (Minobe, 1997, 1999; Chao et al., 2000) and ENSO (2–7 years) (Rasmussen and Carpenter, 1982; Trenberth, 1997). MTM analysis was also conducted on the 28 individual tree-ring chronologies to explore their capacity to capture the PDO- and ENSO-like spectra.

Given the documented relationships between Canadian Prairie hydroclimate and the large-scale teleconnection indices, we also explored the physical dynamics associated with each final principal component. Correlation maps were derived from correlation analysis of $PC1_{final}$ and $PC2_{final}$ and the average December–March (winter) and May–August (summer) gridded 500 hPa geopotential heights, for the 1948–2005 period, using the NCEP Reanalysis data and software (NOAA/OAR/ESRL PSD, Boulder, Colorado, USA; http://www.esrl.noaa.gov/psd/) (Kalnay et al., 1996).

3. Results

Principle component analysis of the 28 standard site chronologies over the common period of AD 1926–2004 produced a first principal component (PC1) that explained 58% of the variance and a second principal component (PC2) that explained 18% of the variance. The reduced $PC1_{final}$ was based on five chronologies which spanned AD 1406–2004 (Appendix A Table A1) and was highly correlated ($r = 0.93$) to the common period PC1 based upon all 28 site chronologies. This reduced $PC1_{final}$ explained 52.5% of the total variance. The reduced $PC2_{final}$ explained 25.4% of the variance and was correlated with the common period PC2 ($r = 0.85$). Hence, the key information from the initial 28 chronologies with a short centennial-length common period is adequately summarized by just five chronologies with a six century time span.

The $PC1_{final}$ study region, consisting of the gridcells whose summer PDSI time series were highly significantly correlated with $PC1_{final}$, coincided with the North and South Saskatchewan River Basins, and the Milk River sub-basin of the Missouri River Basin (Fig. 1a). Linear regression was used to reconstruct the regional average PC1 JJA PDSI using $PC1_{final}$ as the predictor for AD 1406–2004: PC1 JJA PDSI = (−0.5306 + 0.6944*$PC1_{final}$) ($r^2_{adj} = 0.45$; S.E. = 1.26; RE = 0.47) (Fig. 2a). Recent drought intervals from the instrumental period reflected in the tree-ring-derived PC1 JJA PDSI include AD 1918–1926, AD 1930–1941, AD 1956–1963, AD 1983–1989 and AD 2000–2004; hence the tree-ring record is faithfully reproducing the instrumental record (Fig. 2a).

The $PC2_{final}$ study region, consisting of the gridcells whose summer PDSI time series were highly significantly correlated with $PC2_{final}$, included disjunct areas of southern Alberta, Montana, and

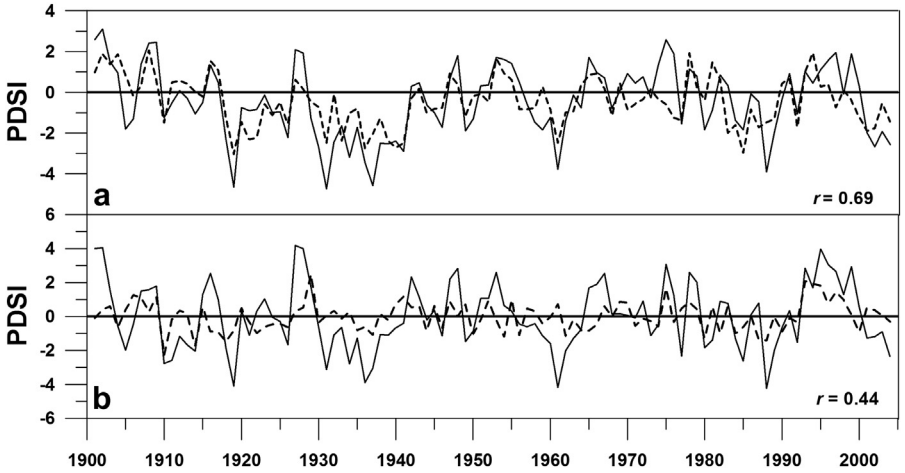

Fig. 2. The reconstructed summer (June–August) Palmer Drought Severity Index regional averages: (a) PC1 JJA PDSI and (b) PC2 JJA PDSI. PC1 JJA PDSI is from the region significantly correlated with $PC1_{final}$ and PC2 JJA PDSI is from the region significantly correlated with $PC2_{final}$, as identified in Fig. 1. The solid line represents the instrumental regional average and the dashed line represents the tree-ring reconstruction inferred from each PC_{final}. Pearson's correlation (r) significant at the 95% confidence level.

western North and South Dakota (Fig. 1b). Linear regression was used to reconstruct PC2 JJA PDSI using $PC2_{final}$ as the predictor for AD 1406–2004: PC2 JJA PDSI = (0.0096 + 0.8103*$PC2_{final}$) (r^2_{adj} = 0.194; S.E. = 1.78; RE = 0.17) (Fig. 2b).

Although we are reconstructing the summer PDSI, there are statistically significant correlations to the winter large-scale circulation patterns and climate. Table 2 shows the Pearson's correlation coefficients (r) for the instrumental JJA PDSI from the $PC1_{final}$ study region and the tree-ring $PC1_{final}$ with regional average winter (December–February) and summer (June–August) precipitation. The strength and value of the correlation between the seasonal precipitation and $PC1_{final}$ are coherent, confirming the potential of using tree-rings to reconstruct summer PDSI values. Also demonstrated is the cumulative lag effect of winter precipitation on the summer PDSI and tree-ring growth which justifies our comparison between winter circulation patterns and the summer PDSI moisture conditions. Composite analysis showed that the recent portion of $PC1_{final}$ contained a strongly significant PDO signal (p = 0.002), but no ENSO signal. The recent portion of $PC2_{final}$ did not contain a PDO signal, but did contain an ENSO signal (p = 0.05). For this reason, we include $PC2_{final}$ in further analysis, although most of the analysis is focused upon $PC1_{final}$ which explains a much greater amount of the total variance.

Table 2
Pearson's correlation coefficients (r) between tree-ring $PC1_{final}$ and the regional instrumental summer (June–August) Palmer Drought Severity Index (JJA PDSI) from the $PC1_{final}$ study region with the winter (December–February) precipitation and summer (June–August) precipitation for AD 1901–2004. Bold denotes significance at the $p \leq 0.01$ level. Significance values were adjusted for autocorrelation according to Dawdy and Matalas (1964).

Variable	Dec–Feb PPT	June–Aug PPT
$PC1_{final}$	**0.33**	**0.42**
Instrumental JJA PDSI	**0.36**	**0.47**

Our reconstruction of summer PDSI (PC1 JJA PDSI) for the North and South Saskatchewan River Basins and Milk River sub-basin over the past six centuries included droughts that were more extreme in severity, intensity, and duration than those during the instrumental period (Table 3). The AD 1858–1872 drought was the most severe and longest, followed by those of AD 1930–1941 and AD 1483–1494 (Table 3 and Figs. 3 and 5a). The drought of AD 1717–1721 ranked only seventh in severity but was the most intense (−2.4). Of the 24 sustained drought events in the full proxy record, eighteen (six) occurred during the positive (negative) PDO phase based on the MacDonald and Case (2005) reconstruction. The dominant PDO phase was consistent between the PDO reconstruction of MacDonald and Case (2005) and the Composite PDO reconstruction of Verdon and Franks (2006) for all droughts except the AD 1755–1761 and AD 1858–1872 episodes. The most severe and longest drought, that of AD 1858–1872, occurred during the positive PDO phase (MacDonald and Case, 2005) and had more occurrences of La Niña than El Niño. The next three droughts, ranked by severity, also occurred during the positive PDO phase, but had more occurrences of El Niño than La Niña. The pre-instrumental period (AD 1406–1871) had 18 droughts, of which 17 had an equal or greater number of La Niñas or neutral phase events than the number of El Niños. Droughts were more likely to be preceded by a La Niña or neutral event rather than an El Niño and there was no consistency for which type of ENSO event occurred as the first year of the drought. During the instrumental period, AD 1872–2005, there were six sustained droughts; all six of which had an equal or greater number of occurrences of La Niñas or neutral events than El Niños. High (low) ENSO variability coincided with 15 (9) drought events, with the five most severe droughts occurring during periods of high ENSO variability (AD 1483–1494, AD 1559–1570, AD 1791–1800, AD 1858–1872, and AD 1930–1941).

Table 3
Sustained drought episodes on the Canadian Prairies in chronological order and their associated duration, severity, rank based on severity, and intensity (severity/duration) over the past six centuries. The type of ENSO event for each year of the drought (beginning with the preceding year) and variance, calculated using a 17-year window (see text and Fig. 3c), was based on the Cook et al. (2008) Niño 3.4 index reconstruction for AD 1300–2006. E = El Niño, L = La Niña, N = neutral, (LV) = low variance, (HV) = high variance. The average PDO phase of the event was based on the MacDonald and Case (2005) PDO reconstruction. If the Composite PDO Index phase (Verdon and Franks, 2006) is not in agreement with the MacDonald and Case PDO phase, this is shown in brackets.

Drought	Duration (years)	Severity	Severity rank	Intensity	ENSO event type (variance)	PDO phase
1472–1481	10	−7.6	14	−0.8	LELLLLEENNN (HV)	+
1483–1494	12	−14.2	3	−1.2	ENEEELLENNELN (HV)	+
1498–1508	11	−8.2	11	−0.7	LEENNLNEELNL (HV)	+
1512–1518	7	−5.8	18	−0.8	ELLLLLNE (LV)	+
1559–1570	12	−12.3	5	−1.0	ENLLNNNELLLLL (HV)	+
1576–1583	8	−6.7	16	−0.8	NLNNLLNEE (LV)	+
1618–1623	6	−4.3	19	−0.7	NELENLL (LV)	−
1626–1630	5	−6.7	17	−1.3	LLNEEE (LV)	−
1645–1654	10	−7.4	15	−0.8	NLENLEEENLL (HV)	−
1682–1688	7	−3.3	24	−0.5	EENLLEEL (LV)	+
1701–1708	8	−7.9	12	−1.0	NNELLLNLN (LV)	−
1717–1721	5	−11.8	7	−2.4	LNENNN (HV)	+
1755–1761	7	−8.8	9	−1.3	LNNLNNLN (HV)	+ (−)
1791–1800	10	−12.7	4	−1.3	LEEENLNNLEE (HV)	+
1811–1815	5	−3.7	23	−0.7	NNLLEE (HV)	−
1842–1847	6	−12.1	6	−2.0	LLLNENN (LV)	+
1850–1854	5	−4.2	21	−0.8	NELENN (LV)	+
1858–1872	15	−19.7	1	−1.3	LELLNLLLNLNNELLL (HV)	+ (−)
1889–1897	9	−7.8	13	−0.9	EELENLNENE (HV)	+
1918–1926	9	−9.5	8	−1.1	LLENNLNNLE (HV)	+
1930–1941	12	−15.6	2	−1.3	LEENNLNNNNLEE (HV)	+
1956–1963	8	−4.2	22	−0.6	LLNENNLEN (LV)	−
1983–1989	7	−8.4	10	−1.2	NELLLEEL (HV)	+
2000–2004	5	−4.3	20	−0.9	LLLNEE (HV)	+[a]

[a] PDO from the instrumental record (http://jisao.washington.edu/pdo/, Mantua et al., 1997).

Along with identifying sustained drought events, runs analysis also categorized 15 sustained abnormally wet periods, which were also compared to the PDO and ENSO reconstructions. There were fewer sustained pluvials than droughts, even given the less stringent definition of pluvial (Table 4). The 18th and 20th centuries each had four pluvial events, demarcating them as the wettest centuries of the entire reconstruction. The most severe pluvial occurred during AD 1826–1830, the second during AD 1668–1676, and the third during AD 1900–1905; the next fourth- through sixth-ranked extreme events occurred during the 18th century. There were seven (eight) events that occurred during the positive (negative) phase of the PDO, based on the MacDonald and Case (2005) reconstruction. The dominant PDO phase was consistent between the MacDonald and Case (2005) and the Composite PDO reconstructions for all pluvials except that of AD 1826–1830. Pluvials typically had more occurrences of the La Niña or neutral events than El Niño events. However, the frequency of El Niño was higher during the positive PDO phase pluvials of AD 1550–1554 and AD 1900–1905. There were no prevailing type of ENSO event

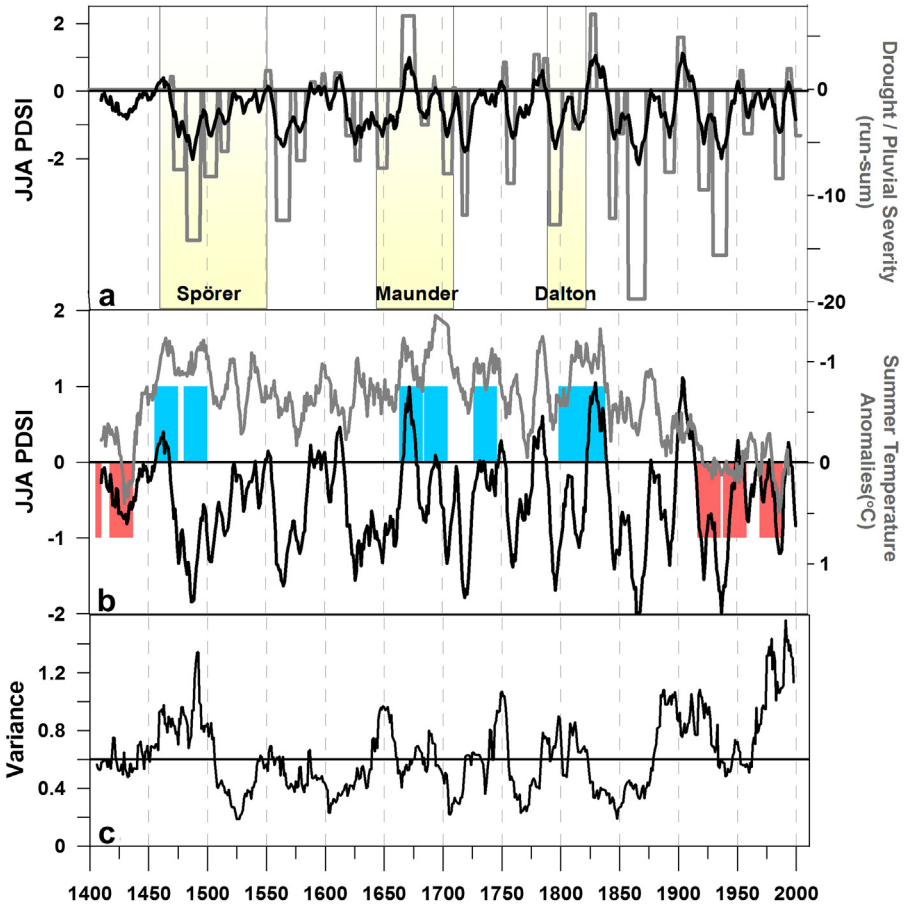

Fig. 3. (a) Runs analysis of the summer Palmer Drought Severity Index reconstruction (PC1 JJA PDSI) for the past six centuries. PC1 JJA PDSI (solid black line) smoothed by a 9-year running average. The grey bars denote the drought/pluvial severity (run-sum), and the light yellow panels represent approximate timing and duration of solar minima (Spörer, Maunder, and Dalton, respectively). (b) Comparison of the summer Palmer Drought Severity Index reconstruction (PC1 JJA PDSI) to the Luckman and Wilson (2005) summer temperature reconstruction. The PC1 JJA PDSI (black line) is smoothed by a 9-year running average. The reconstructed summer temperature anomalies (°C) (grey line) are inverted, and shown relative to their 1900–1980 mean. The red (blue) bars represent extreme 20 year periods (inverted) of warm (cool) intervals, relative to 1900–1980 mean. (c) Variance plot of the Cook et al. (2008) reconstructed Niño 3.4 Index using a sliding 17-year window (value assigned to centre year of the window). The solid black line represents the average variance (0.6) over the entire reconstruction length (AD 1300–1979). (For interpretation of the references to colour in this figure legend, the reader is referred to the web version of this article.)

that preceded the pluvials; four events were preceded with a La Niña, six with a neutral event, and five with an El Niño event. Also, there was no consistent type of ENSO event during the first year of the pluvials. ENSO variability appears to have little impact; eight pluvials were associated with low variability, including the two most extreme events, and seven events with high variability.

The strength and sign of the running correlations between the final tree-ring principal components and the PDO and ENSO

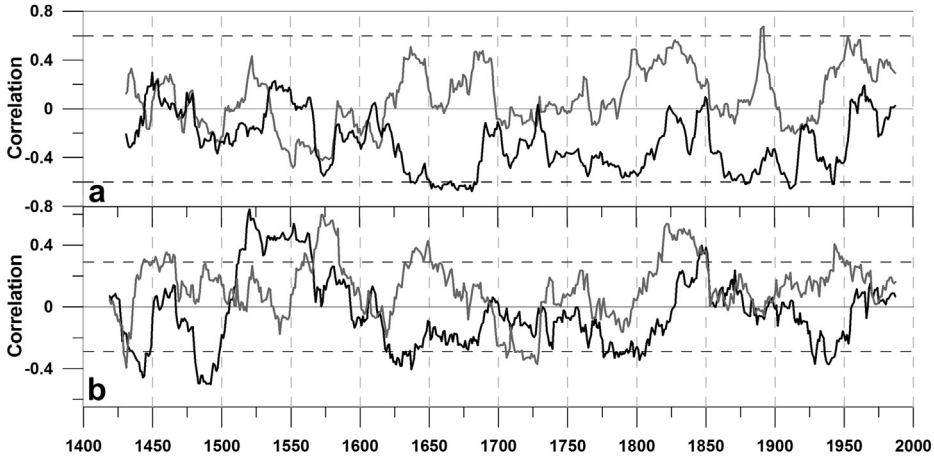

Fig. 4. (a) Correlation plot between the MacDonald and Case (2005) reconstructed PDO index and $PC1_{final}$ (black line) and $PC2_{final}$ (grey line), using a 31-year window (value assigned to centre year of the window). (b) Correlation plot between the Cook et al. (2008) reconstructed Niño 3.4 index and $PC1_{final}$ (black line) and $PC2_{final}$ (grey line). The horizontal dashed line corresponds to $p \leq 0.1$.

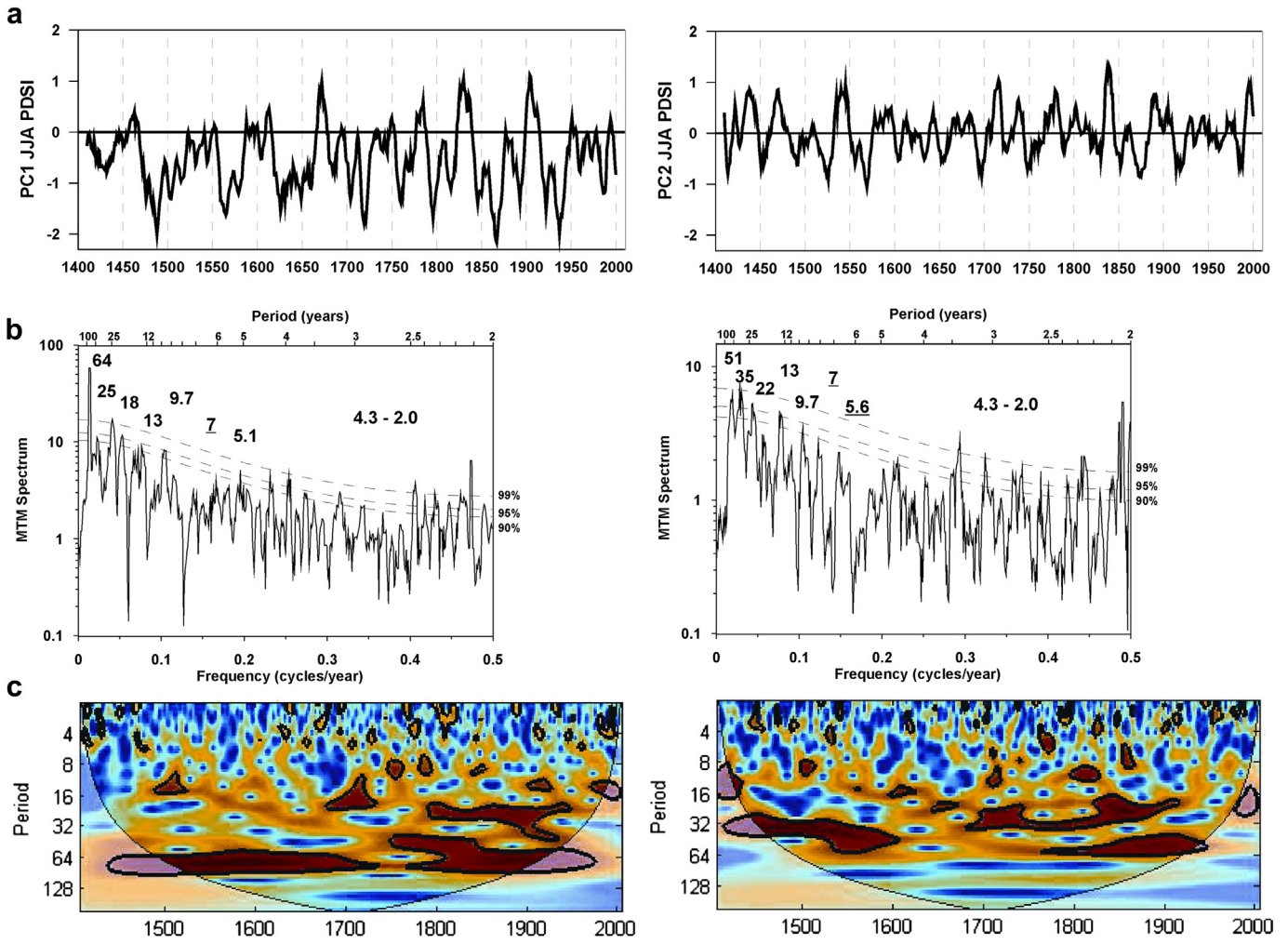

Fig. 5. (a) The reconstructed summer (June–August) Palmer Drought Severity Index regional averages: PC1 JJA PDSI (left panel) and PC2 JJA PDSI (right panel). The reconstructions span AD 1406–2004, and are smoothed by a 9-year running average. (b) Their MTM spectra and significance levels (smoothed dotted curves). The bold values are periods (in years) significant at the $p \leq 0.1$ level and the underlined values are periods nearly significant. (c) Their Morlet wavelet evolutionary spectra, with the heavy black line showing significance at the $p \leq 0.1$ level.

Table 4
Sustained pluvial episodes on the Canadian Prairies in chronological order and their associated duration, severity, rank based on severity, and intensity (severity/duration) over the past six centuries. The type of ENSO event for each year of the pluvial (beginning with the preceding year) and variance, calculated using a 17-year window (see text and Fig. 3c), was based on the Cook et al. (2008) Niño 3.4 index reconstruction for AD 1300–2006. E = El Niño, L = La Niña, N = neutral, (LV) = low variance, (HV) = high variance. The average PDO phase of the event was based on the MacDonald and Case (2005) PDO reconstruction. If the Composite PDO Index phase (Verdon and Franks, 2006) is not in agreement with the MacDonald and Case PDO phase, this is shown in brackets.

Pluvial	Duration (years)	Severity	Severity rank	Intensity	ENSO event type (variance)	PDO phase
1469–1471	3	1.2	13	0.4	LELL (HV)	+
1550–1554	5	1.8	9	0.4	EEENEE (HV)	+
1588–1592	5	0.7	14	0.1	NNLNEL (LV)	−
1598–1600	3	1.5	12	0.5	ENNL (LV)	+
1609–1614	6	1.5	11	0.3	ENENNLN (LV)	+
1668–1676	9	6.9	2	0.6	LLNLELLENL (LV)	−
1709–1711	3	0.1	15	0.0	NLEN (LV)	−
1752–1754	3	2.6	6	0.9	NLLL (HV)	−
1778–1782	5	3.3	4	0.7	LLNELL (LV)	−
1786–1790	5	2.9	5	0.7	LLNELL (HV)	−
1826–1830	5	7.0	1	1.4	ELEENL (LV)	− (+)
1900–1905	6	4.9	3	0.8	NEENELE (HV)	+
1907–1909	3	1.7	10	0.6	NNNL (HV)	+
1953–1955	3	1.8	8	0.6	NLLL (LV)	−
1993–1996	4	2.0	7	0.5	EENEL (HV)	+

reconstructions vary throughout AD 1406–2004 (Fig. 4). The running correlations of $PC1_{final}$ and $PC2_{final}$ with the PDO reconstruction were inconsistent with the historical relationship between the PDO and Canadian Prairie moisture (Fig. 4a). $PC1_{final}$ predominantly had a negative relationship with the PDO reconstruction, but with weak positive correlations dispersed throughout the reconstructed time period. Significant ($p \leq 0.10$) negative correlations occurred during AD 1640–1690, AD 1865–1880, AD

1910–1920, and ~AD 1945. $PC2_{final}$ overall had a weak non-significant positive correlation with the PDO reconstruction and interspersed periods of weak negative correlations. The running correlations of $PC1_{final}$ and $PC2_{final}$ with the ENSO reconstruction also oscillated between significantly positive periods and significantly negative periods (Fig. 4b).

The majority of sustained droughts (*e.g.*, AD 1559–1583, AD 1717–1721 and AD 1858–1872) occurred during relatively warm periods in the Luckman and Wilson (2005) summer temperature reconstruction (Fig. 3). All of the 20th century droughts occurred during, or partially overlapped, an extreme warm interval. However, the droughts of the mid-to-late AD 1400's and early AD 1500's, and AD 1811–1815 occurred within the Spörer and Dalton solar minima, and therefore during three of the most extreme cool intervals of AD 1456–1475, AD 1481–1500, and AD 1799–1818. Overall, the sustained pluvial periods tended to occur during cool periods; five (AD 1469–1471, AD 1668–1676, AD 1778–1782, AD 1786–1790 and AD 1826–1830) were during cool intervals and the AD 1709–1711 pluvial followed the Maunder minimum. Although no pluvial occurred during AD 1724–1750 according to our definition, it was wet; and according to Luckman and Wilson (2005), AD 1727–1746 was an extreme cool interval. The early 20th century AD 1900–1910 pluvial was relatively warm compared to the entire (AD 1406–2006) time series mean; however, it was relatively cool compared to the AD 1900–1980 reconstruction mean, reflecting the increasing summer temperature since the AD 1850s. The AD 1953–1956 pluvial was the only one that occurred during an extreme warm interval.

Multi-taper spectral analysis of $PC1_{final}$ over its six century time series showed that it contained the characteristic spectrum of the PDO: the lowest frequency pentadecadal periodicity, the low-frequency bidecadal periodicity, and the higher frequency variability in the 2–7 year ENSO band (Fig. 5) (Minobe, 1997). Evolutionary wavelet plots showed that low frequency variability was reduced during the last half of the AD 1700s (Fig. 5c) when temperatures alternated between cool and warm decades (Luckman and Wilson, 2005). Similarly, $PC2_{final}$ also contained some low frequency pentadecadal (~50 year) and bidecadal (22–35 years) periodicity, but more of the high frequency variability in the ENSO bands than $PC1_{final}$ did (Fig. 5b and c). Both principal components captured a significant 13-year band of variability (Fig. 5b). From MTM spectral analysis of each of the 28 tree-ring site chronologies, we concluded that those with sufficient length (greater than 150 years) detected all three PDO frequency bands and the short chronologies (less than 150 years) detected the ENSO and the bidecadal PDO frequency bands (results not shown). Hence, the importance of the PDO as a regional hydroclimatic forcing, evident in the instrumental record, is demonstrated to have held during the Little Ice Age.

The spatial correlation plots of $PC1_{final}$ and $PC2_{final}$ with the average gridded December–March (winter) and May–August (summer) seasonal 500 hPa heights for AD 1948–2004 are shown in Fig. 6. Negative (positive) correlations imply high (low) 500 hPa heights associated with droughts; the opposite correlations are associated with pluvials. During the winter season, the $PC1_{final}$ drought conditions are associated with a ridge of high pressure originating off the west coast of North America that extends over the Pacific Northwest and south over the southeastern United States. Low pressure is located over the North Pacific Ocean and off the west coast of Mexico. During the summer season, the $PC1_{final}$ drought conditions are associated with high pressure located over western North America that encompasses the study region; low pressure is located in the eastern North Pacific Ocean and continues north of the high pressure system and then south along the eastern North America. The $PC2_{final}$ drought conditions are associated with high pressure off the west coast of North America and over the Gulf of Mexico; low pressure is found over northern Canada, off the east coast of Canada, and over the tropics during the winter season (Fig. 6). During the summer season the high/low pressure areas are shifted westward relative to their winter positions, with the regions over eastern Canada and the tropics heightened in amplitude and the others weakened in amplitude.

4. Discussion

In this study we reconstructed the summer Palmer Drought Severity Index (PDSI) for the northwestern Great Plains over the last six centuries (Figs. 3 and 5a). This study's analysis of sustained drought and pluvial episodes demonstrates the complexity of the linkages between the large-scale teleconnections, specifically the PDO and ENSO, and the associated hydroclimate variability in the eastern Rocky Mountains of southern Alberta and northern Montana (Fig. 1). Of the 24 sustained drought episodes in the full proxy record, three-quarters occurred during a reconstructed positive PDO phase (MacDonald and Case, 2005), demonstrating the importance of this PDO phase as an antecedent for regional multi-annual drought prior to the onset of instrumental records. Sustained pluvials were equally likely in either PDO phase. Unexpectedly, sustained drought intervals contained more reconstructed La Niña events or neutral events than El Niño events (Cook et al., 2008), as did sustained pluvial intervals. However, ENSO variability tended to be higher during multi-annual droughts, but not during the sustained pluvials. Comparison with an independent summer temperature reconstruction (Luckman and Wilson, 2005) confirms the existence of cold multi-annual droughts during the Little Ice Age, although the majority of the sustained droughts occurred in relatively warm intervals.

This study expands upon and provides a more detailed analysis than the North America Drought Atlas (Cook et al., 2004, 2007) which used a network of tree-ring chronologies to reconstruct the PDSI over Canada, the United States and Mexico, covering the past 1000 years or more in some regions. Their PDSI reconstruction grid over western Canada was based on smaller sample depth and a smaller number of chronologies that were not all explicitly collected from moisture sensitive sites, unlike our reconstruction. Thus, our reconstruction of PDSI over the northwestern Great Plains is more robust than the northern margins of the Cook et al. (2004, 2007) grid.

Our study focused on identifying sustained drought and pluvial episodes on the Canadian Prairies and exploring possible forcing mechanisms for these extreme events. Today, regional precipitation is nearly evenly split into warm season (May–September) rain and cold season (November–April) snowpack. Snowpack amount has a disproportionate impact on soil moisture recharge, as it does on surface water and groundwater recharge (Hamlet et al., 2007; Pomeroy et al., 2007; Pham et al., 2009). Hence, antecedent winter precipitation has a significant impact on the spring/summer soil moisture conditions in these northern latitudes. This prompted our hypothesis that decreases in snowpack have been an important antecedent for periods of sustained drought in the recent past (and conversely for increased snowpack and pluvials). Certainly, both the instrumental PDSI and our tree-ring first principal component ($PC1_{final}$) are strongly positively correlated with both winter and summer seasonal precipitation over the Canadian Prairies (Table 2). Winter snowpack is, in its turn, strongly influenced by climate oscillations such as the PDO and ENSO, which typically have their strongest manifestations in winter. Hence, the PDO and ENSO states are strongly linked to sustained regional hydroclimate extremes. Unfortunately, there is no snowpack reconstruction for our study region. Pederson et al. (2011) reconstructed northern Rocky

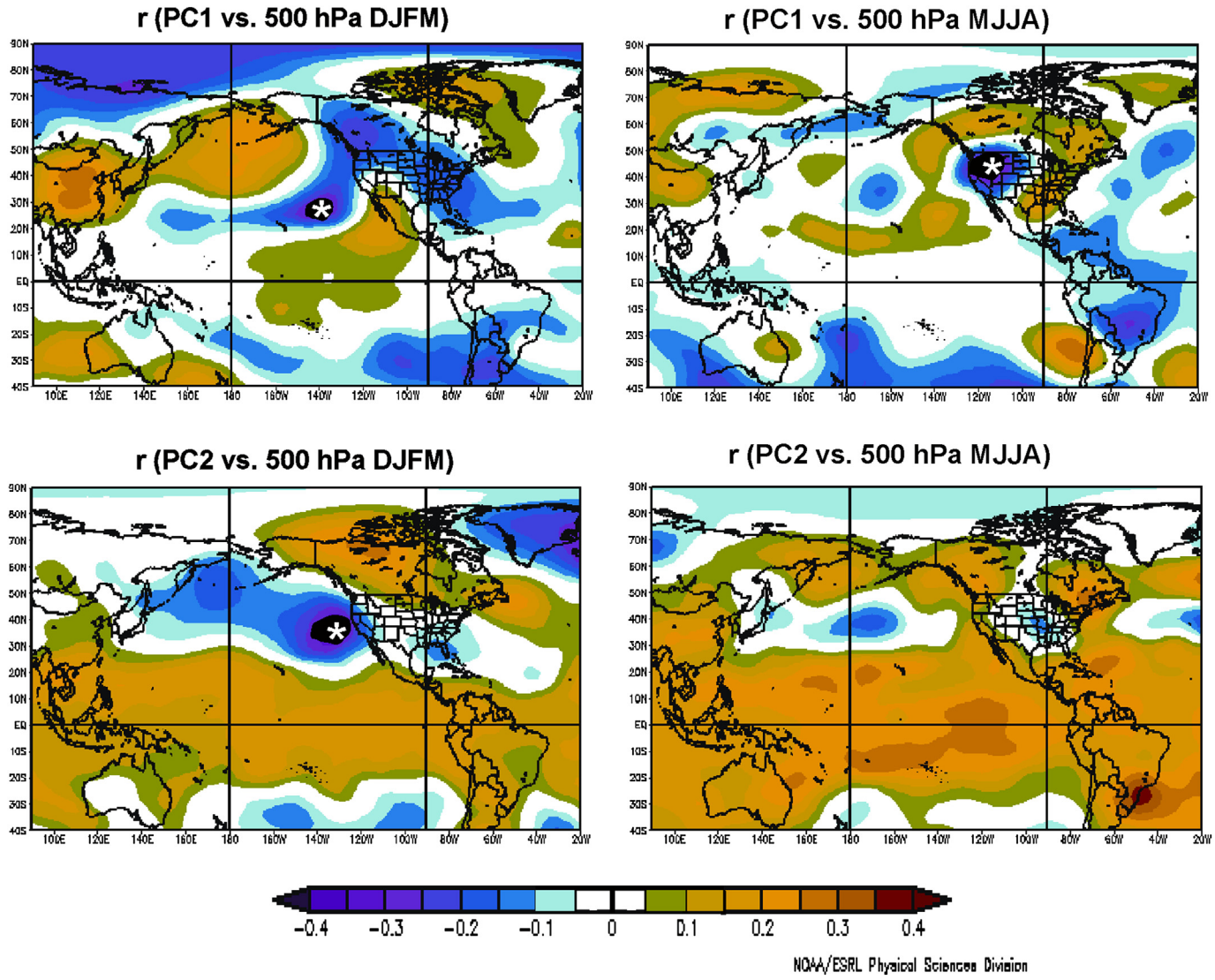

Fig. 6. Correlation maps of $PC1_{final}$ and $PC2_{final}$ with the observed 500 hPa geopotential heights (Kalnay et al., 1996) averaged over the previous December–current March and current May–August season, for AD 1948–2004. Significant correlations at the $p \leq 0.1$ level are demarcated by black fill with a white asterisk inset. Images produced by the software provided by the NOAA/ESRL Physical Sciences Division, Boulder, Colorado (http://www.esrl.noaa.gov/psd/).

Mountains April 1 snow water equivalence (SWE), but their study region was to the west and south of ours, except for a single site out of 66. Using a subset of our tree-ring chronologies, St. George et al. (2009, 2010) developed a tree-ring record of PDSI anomalies across the Canadian Prairie Provinces. They found no apparent relationship between the western Canadian tree-ring chronologies and the instrumental period PDO and the Cold Tongue Index (an ENSO metric). However, composite analysis of our $PC1_{final}$ found a PDO signal present in the instrumental period; and our $PC2_{final}$ contained an instrumental ENSO signal. Our results are consistent with the South Saskatchewan River reconstruction of Axelson et al. (2009).

We also compared our summer PDSI reconstruction to another regional climate reconstruction by Edwards et al. (2008) of growing season atmospheric relative humidity (RH) from the adjacent Columbia Icefield area in the eastern Rocky Mountains, over the past 1000 years, based upon stable isotopes from tree-rings. By comparing their RH reconstruction to previous temperature and streamflow reconstructions, Edwards et al. (2008) summarized recent glacial expansion as occurring during ~AD 1450–1500, ~AD 1590–1610, ~AD 1700–1710, and ~AD 1810–1860, periods that their stable isotope records showed to be cold and dry. The declines in RH during ~AD 1450–1500 and ~AD 1810–1860 closely align with cold droughts in our summer PDSI reconstruction; the onset of each period is a pluvial, corresponding to a higher RH, which then progresses to drought conditions, corresponding to lower RH levels (Fig. 3). The sharp temporary increase in RH at ~AD 1600 corresponds to a pluvial in our reconstruction and the steep decline in RH at ~AD 1700–1710 also corresponds to a drought event.

Edwards et al. (2008) hypothesized that the relatively cold dry conditions of the Little Ice Age (~AD 1530–1890) were due to an intensified meridional circulation and strengthened Aleutian Low. This resulted in a lack of warm Pacific air masses relative to cool Arctic air masses, as suggested by the suppressed PDO variability (MacDonald and Case, 2005) and negative North Atlantic Oscillation/Arctic Oscillation (NAO/AO) index (Wallace and Gutzler, 1981; Cook et al., 2002). Outbreaks of warm Pacific air masses and enhanced North Pacific Ocean variability (MacDonald and Case, 2005) are most likely associated with the pluvial events during this period. The most recent drought of AD 2000–2004 was also anomalously cool compared to previous droughts in the instrumental record (Bonsal et al., 2011); however, cold droughts

were more common during the Little Ice Age, as is shown by our study.

Spectral analysis of our summer PDSI reconstruction also demonstrated the influence of winter season climate variability associated with the large-scale circulation patterns. MTM and wavelet analysis revealed dominant modes of variability in the tree-ring series at the pentadecadal and bidecadal periodicities characteristic of the PDO and at the 2–7 years band characteristic of ENSO (Fig. 5). The NAO also influences northwestern North American hydroclimate (Bonsal et al., 2001; St. Jacques et al., 2010); however, to differentiate its frequency (2–10 years) (Hurrell and Deser, 2009) from the ENSO frequency is problematic. The lack of low frequency variability between AD 1700 and AD 1850, as shown in the wavelet analysis, corresponds to a northward migration of the Inter-tropical Convergence Zone (Sachs et al., 2009). Temperatures around the latter half of the 1700s alternated between cool and warm decades (Luckman and Wilson, 2005), and may have also contributed to the lack of low-frequency variability.

The varied temporal correlations between our reconstructed summer PDSI and the reconstructed PDO index potentially demonstrate the inconsistent modulation of the summer PDSI by this teleconnection (Fig. 4). During the periods of significant correlation, the hydroclimatic impact of the PDO is carried over from winter to spring/summer. We speculate that the periods of non-significant or even positive correlation are explained by the lack of carry over from the winter season hydroclimatic signal, particularly if opposite correlations occurred during the following growing season. For example, weak positive correlations could be found during a year with a negative winter PDO index, or weakened Aleutian Low, and increased winter precipitation; however this above average snowpack may not be followed by the spring/summer precipitation required during the growth season, or warm temperatures may result in enhanced evapotranspiration and produce drought conditions. Based on this example and the ability of tree-rings to capture dry years better than wet years, we would anticipate that the reconstructions would capture the positive phase of the PDO and enhanced Aleutian Low conditions better than the opposite conditions.

The fingerprint of ENSO also manifested in our summer PDSI reconstruction. El Niño is linked with both winter and summer seasonal drought in the northern Prairies (Shabbar et al., 1997; Bonsal and Lawford, 1999; Bonsal et al., 2006; Shabbar, 2006). The winter 500 hPa heights associated with $PC1_{final}$ drought conditions are associated with a deepened Aleutian low and a stronger northward flow (Fig. 6). These conditions resemble an El Niño-like atmospheric circulation (Trenberth and Hurrell, 1994; Lau, 1997; Bonsal et al., 2001; Yu and Zwiers, 2007). The summer meridional circulation pattern is concurrent with dry periods (Fig. 6) and the common amplified mid-tropospheric ridge and trough pattern, which causes the western directed flow northward of the Prairie region (Bonsal et al., 1999).

Although El Niño, rather than La Niña, is associated with Canadian Prairie drought in the instrumental period, the connection between La Niña events and reconstructed summer droughts may not be that uncommon. Since the onset of SST observations, five multi-year mid-latitude drought events in North America that affected the Canadian Prairies (AD 1856–1865, and the 1870s, 1890s, 1930s, and most of the early 21st century) have been accompanied by persistent La Niña-like SST conditions (Fye et al., 2003; Herweijer et al., 2006; Seager, 2007; Woodhouse et al., 2012).

The instrumental summer JJA PDSI regional average and the tree-ring $PC1_{final}$ are linked to both winter and summer climate conditions, therefore it is difficult to separate winter and summer signals in any annual PDSI signal (Table 2). The period of March through May is typically the ENSO transition period (Trenberth, 1997). If an El Niño event finished during a given winter and then the tropical Pacific Ocean transitioned into La Niña during the summer, then an annual PDSI record would capture a mixed signal: El Niño-related decrease in winter precipitation (Shabbar et al., 1997), and then La Niña-related increase in summer precipitation (Bonsal and Lawford, 1999) (and similarly for the transition between La Niña to El Niño). This connection to both seasonal climates could explain the uncertainty around El Niño versus La Niña events being associated with sustained summer drought occurrences. Exploring the separate early/late wood thicknesses and analyzing each seasonal chronology for the dominate moisture signal may help differentiate this mixed winter and summer season signal (Vanstone and Sauchyn, 2010).

The winter 500 hPa heights centres-of-action pattern (*i.e.*, the high off the Californian coast) associated with $PC2_{final}$ drought conditions (Fig. 6) is a distinct feature of La Niña (Diaz et al., 2001), along with the depressed 500 hPa heights at longitudes in the tropical and subtropical latitudes. Because of this and the composite analysis results, we interpret $PC2_{final}$ as an independent ENSO teleconnection signal. During the summer these centres-of-action are shifted westward, with weaker amplitudes, relative to their winter positions (Fig. 6). Although $PC2_{final}$ is capturing a relatively small portion of the overall hydroclimatic variability of the study region, it does highlight the non-stationary temporal relationship and spatial variability between the hydroclimate and ENSO (Fig. 4b). The non-stationary relationship also exists over western Montana in the instrumental record (Wise, 2010). The weak ENSO signal in the tree-rings may be explained by the sporadic occurrence of ENSO events or by the variable antecedent soil moisture conditions.

Although the PDO and ENSO are predominantly winter signals affecting snowpack, various linkages have been made between the summer Pacific Ocean and Canadian Prairie summer climate conditions via the atmospheric Pacific North American (PNA) pattern. The PNA is one of the most prominent modes of low-frequency atmospheric variability in the Northern Hemisphere extra-tropics and is associated with strong fluctuations in the strength and location of the East Asian jet stream (Wallace and Gutzler, 1981). Spring and summer precipitation have been linked to the PNA (Knox and Lawford, 1990; Bonsal et al., 1999). In turn, the PNA is influenced by the PDO (Bonsal and Shabbar, 2011) and ENSO (Renwick and Wallace, 1996). Typically with the positive phase of the PNA, there are also more occurrences of the positive PDO phase and El Niño events. The PNA pattern exhibits inter-decadal variability and is related to the strength of the Aleutian Low.

This study focused on exploring the extreme conditions of sustained drought and pluvial episodes using tree-rings as proxies for moisture conditions. Although other researchers have used these methods for similar purposes, it is important to acknowledge their limitations in capturing the full variability, specifically in the case of precipitation, of extreme moisture events. Tree growth is subject to its most limiting factor, typically the availability of either water or heat. Therefore, narrow tree-rings record deficits, such as droughts or cold conditions, more clearly than surpluses and this must be kept in mind when rating the severity and intensity of the pluvial episodes. This limitation results in tree-ring proxy climate reconstructions unable to capture the full range of variance for the chosen site. Rarely is more than 60% of the variance captured, with 40–50% being the more common level of calibrated variance (Sauchyn and Beaudoin, 1998; Collins et al., 2002; Hughes, 2002; St. George and Nielsen, 2002; Watson and Luckman, 2005a). We address this limitation by using a network of moisture-sensitive trees over a large spatial area (Peterson and Peterson, 2001; Gray

et al., 2006). This increases the confidence that the dominant climate signal is captured and robustly reconstructed.

Further problems with tree-ring climate reconstructions arise due to variable-length lags and carry-overs of antecedent conditions from both soil moisture reserves and tree physiological responses. For instance, we found that the drought of AD 2000–2001 did not exhibit as pronounced a negative anomaly, relative to other 20th century droughts, such as that of AD 1936–1937 (St. George et al., 2009), even though AD 2000–2001 was deemed the most intense two-year drought in the western prairies during the last 100 years (Sauchyn et al., 2003; Lui et al., 2004). The absence of an extremely narrow AD 2001 tree-ring may be explained by the previous years' carry-over of moisture (Fritts, 1976); the AD 2000–2001 drought was preceded by eight wet years, unlike the AD 1936–1937 drought.

There are also problems with using the PDSI as a drought metric in this region, as it treats all precipitation as rainfall and does not carry over water stored as snow beyond its impact on the monthly water balance (Alley, 1984; St. George et al., 2010). This problem is potentially illustrated by the following: Western North American hydroclimatology is strongly influenced by the PDO/ENSO dipole (*e.g.*, Redmond and Koch, 1991; Gershunov and Barnett, 1998; Wise, 2010). When the PDO is negative and/or a La Niña occurs, northwestern North America is wet and the American Southwest and northern Mexico are dry and vice-versa for the positive PDO and El Niño. Severe moisture extremes tend to occur in one pole at a time, but not in the other (*e.g.*, Cook et al., 2007; Woodhouse et al., 2012). A problem with the PDSI is the weak northwestern pole relative to the southwestern pole shown in a composite analysis plot of ENSO's effect on instrumental North American PDSI shown in St. George et al. (2010); whereas similar analysis of ENSO's effect on instrumental North American precipitation shows an equally strong northwestern pole (Redmond and Koch, 1991; Wise, 2010). However, regardless of exactly what it is called, the first principal component of our set of tree-ring chronologies ($PC1_{final}$) contains a primary drought signal as the sites were explicitly chosen to be water-stressed (which was confirmed by correlation analysis with climate variables, results not shown). Hence, our 600-year tree-ring record contains a regional sustained drought record and the analysis of its forcings is meaningful, despite the problems with the PDSI.

Future research could include comparing Canadian Prairie tree-ring derived drought reconstructions to other large-scale climate factors such as the PNA or the North Pacific Index (NPI) as other metrics of Pacific Ocean climate variability. The NPI is a measure of the intensity of the Aleutian Low, which is a possible driving mechanism of the PDO. Rather than using the PDO and ENSO as the only metrics for measuring the Pacific climate variability, the PNA and the NPI could also be considered as other key physical variables (IPCC4, 2007). However, robust, long proxy-derived reconstructions of the PNA and NPI are not yet available.

A scientific basis for adapting current water infrastructure, policy, and management to uncertainty in the future climate system due to global warming involves an understanding of historical climate variability and the drivers of climatic extremes (Biondi et al., 2005). Future patterns of SST anomalies in the extra-tropical North Pacific Ocean will likely include a shift circa AD 2050 in the decadal time-scale variability, impacting oceanic processes by changing the gyre evolution and the associated change in storm tracks (Trenberth, 1990; IPCC4, 2007; Overland and Wang, 2007; Lapp et al., 2012). Increased ENSO variance during the 20th century roughly coincides with an increase in Western Pacific Ocean warm-pool temperature (Newton et al., 2006). Assuming that the warm-pool SSTs can be attributed to global warming, this supports the view that anthropogenic global warming tends to strengthen the ENSO variability (Sun, 2003). Given our results of the importance of North Pacific Ocean variability and high ENSO variance in contributing to Canadian Prairie drought over the past 600 years, we conclude that near future drought and flood severity and variability may surpass the instrumental and reconstructed records (St. Jacques et al., 2013). This study demonstrates the value of reconciling short-term instrumental records (~100 years or less) with longer-term paleo-data to derive insights into natural climate variability and to improve our understanding of climate related risk (Verdon-Kidd and Kiem, 2010; Kiem and Verdon-Kidd, 2011).

Acknowledgements

We thank the World Data Center for Paleoclimatology for their archived data. The NCEP Reanalysis data was provided by the NOAA/OAR/ESRL PSD, Boulder, Colorado, USA (http://www.esrl.noaa.gov/psd/). This research was funded by the Natural Sciences and Engineering Research Council of Canada. We thank two anonymous reviewers whose thoughtful comments greatly improved this manuscript.

Appendix A

Table A1
The 28 standard tree-ring chronologies used in this study and their details. The chronologies were collected by the University of Regina Tree-Ring Laboratory. The expressed population signal (EPS) measures the ability of each record to represent the ideal population signal, and the between-tree correlation (R_bar) is the mean correlation between all ring width records within a site. Median series length is the median number of annual rings contained by the tree-ring samples from an individual site. SSS >0.85 is the earliest year that the chronology is able to estimate at least 85% of the original signal, derived from all trees within the stand. Sens is mean sensitivity of the residual chronology. Not available is denoted by *na*. *Picea glauca* (PCGL); *Pinus contorta* (PICO); *Pinus flexilis* (PIFL); *Picea glauca* (PIGL); *Pseudotsuga menziesii* (PSME). *denotes the five longest chronologies used in the reconstructions.

Site name	Species	Lat (°N)	Long (°W)	EPS	R_bar	Median	Trees	Cores	First year	Last year	SSS >0.85	Sens
Beaver Creek, AB	PSME	49.8	−113.9	0.93	0.56	275	10	23	1592	2006	1624	0.237
Beaver Dam Creek, AB	PSME	49.9	−114.2	0.97	0.55	345	29	42	1482	2004	1526	0.279
Buhrman, AB	PIFL	49.1	−113.6	0.93	0.31	83	27	34	1796	2007	1896	0.270
Boundary, AB	PSME	49.1	−114.0	0.95	0.41	198	27	45	1759	2005	1780	0.200
Burles Ridge, AB	PSME	49.7	−114.1	0.88	0.57	163	5	7	1768	2004	1830	0.319
Beauvais Lake, AB	PSME/PIFL	49.4	−114.1	0.96	0.40	257	17	34	1627	2003	1701	0.219
Cabin Creek, AB*	PSME	49.7	−114.0	0.99	0.67	406	32	40	1375	2004	1406	0.369
Callum Creek, AB	PSME	50.0	−114.2	0.97	0.56	288	25	35	1572	2004	1634	0.250
Cypress Hills, SK	PICO	49.7	−110.0	0.92	0.26	99	34	40	1872	2001	1885	0.152
Crandell Mountain, AB	PSME	49.1	−113.9	0.89	0.40	227	10	30	1450	2005	1457	0.175

Table A1 (*continued*)

Site name	Species	Lat (°N)	Long (°W)	EPS	R_bar	Median	Trees	Cores	First year	Last year	SSS >0.85	Sens
Dutch Creek, AB	PSME	49.9	−114.4	0.98	0.64	244	34	42	1618	2004	1620	0.310
Douglas Fir Ecological Area, AB	PSME	52.2	−116.4	0.98	0.60	294	35	49	1472	2007	1587	0.332
Emerald Lake, AB	PIFL	49.6	−114.6	0.93	0.29	270	30	39	1450	2004	1591	0.215
Hawkeye Mesa, AB	PIFL	49.7	−113.8	0.94	0.41	171	23	59	1542	2007	1641	0.245
Little Bob Creek, AB	PSME	49.9	−114.2	0.98	0.63	307	32	45	1509	2004	1579	0.322
Oldman River, AB	PSME	49.9	−114.2	0.94	0.57	202	12	26	1534	2003	1597	0.374
Oldman River, AB*	PIFL	49.8	−114.2	0.98	0.50	284	48	90	1203	2007	1364	0.329
Ridge Crest, AB	PSME	49.9	−114.3	0.93	0.54	167	10	10	1797	2003	1810	0.209
Siffleur Ridge, AB*	PIFL	52.0	−116.4	0.98	0.56	244	35	62	1018	2008	1028	0.355
Stoney Indian Park, AB	PSME	51.1	−115.0	0.98	0.68	270	19	22	1597	2003	1637	0.296
South Milk River, MT	PIFL	48.7	−113.3	0.82	0.23	79	13	13	1892	2007	1926	0.183
Tower Ridge, AB	PCGL	51.1	−114.4	0.98	0.41	131	70	93	1315	1992	1602	0.267
Two O'Clock Creek, AB	PSME	52.1	−116.4	0.98	0.56	411	24	38	1496	2007	1500	0.338
Wildcat Hills, AB*	PSME	51.3	−114.7	0.98	0.72	300	21	48	1341	2006	1351	0.419
Ward Creek, AB	PSME	50.1	−114.2	0.97	0.55	169	22	32	1708	2005	1724	0.165
Whirlpool Point, AB*	PIFL	52.0	−116.5	0.96	0.59	261	16	32	1062	2007	1160	0.395
White Rabbit Creek, AB	PIFL	52.1	−116.4	0.98	0.68	266	24	38	1555	2008	1559	0.366
West Sharples Creek, AB	PSME	49.9	−114.1	0.99	0.55	360	55	63	1525	2004	1562	0.291

References

Alley, W.M., 1984. The Palmer Drought Severity Index, limitations and assumptions. Journal of Climate and Applied Meteorology 23, 1100–1109.

Ault, T.R., St. George, S., 2010. The magnitude of decadal and multidecadal variability in North American precipitation. Journal of Climate 23, 842–850.

Axelson, J.N., Sauchyn, D.J., Barichivich, J., 2009. New reconstructions of streamflow variability in the South Saskatchewan River Basin from a network of tree ring chronologies, Alberta, Canada. Water Resources Research 45, W09422.

Batjes, N.H. (Ed.), 2000. Global Data Set of Derived Soil Properties, 0.5-Degree Grid (ISRIC-WISE). [Global Data Set of Derived Soil Properties, 0.5-Degree Grid (International Soil Reference and Information Centre – World Inventory of Soil Emission Potentials)]. Oak Ridge National Laboratory Distributed Active Archive Center, Oak Ridge, Tennessee, U.S.A. Data set. Available on-line: http://www.daac.ornl.gov.

Biondi, F., Gershunov, A., Cayan, D.R., 2001. North Pacific decadal climate variability since 1661. Journal of Climate 14, 5–10.

Biondi, F., Kozubowski, T.J., Panorska, A.K., 2005. A new model for quantifying climate episodes. International Journal of Climate 25, 1253–1264.

Bonsal, B.R., Lawford, R.G., 1999. Teleconnections between El Niño and La Niña events and summer extended dry spells on the Canadian Prairies. International Journal of Climatology 19, 1445–1458.

Bonsal, B., Shabbar, A., 2011. Large-scale Climate Oscillations Influencing Canada, 1900–2008. Canadian Biodiversity: Ecosystem Status and Trends 2010, Technical Thematic Report No. 4. Canadian Councils of Resource Ministers, Ottawa, ON. iii + 15 pp.

Bonsal, B.R., Zhang, X., Hogg, W.D., 1999. Canadian Prairie growing season precipitation variability and associated atmospheric circulation. Climate Research 11, 191–208.

Bonsal, B.R., Shabbar, A., Higuchi, K., 2001. Impact of low frequency variability modes on Canadian winter temperature. International Journal of Climatology 21, 95–108.

Bonsal, B.R., Prowse, T.D., Duguay, C.R., Lacroix, M.P., 2006. Impacts of large-scale teleconnections on freshwater-ice break/freeze-up dates over Canada. Journal of Hydrology 330, 340–353.

Bonsal, B.R., Wheaton, E.E., Chipanshi, A., Lin, C., Sauchyn, D.J., Wen, L., 2011. Drought research in Canada, a review. Atmosphere-Ocean 4, 303–319. http://dx.doi.org/10.1080/07055900.2011.555103.

Briffa, K., Jones, P.D., 1990. Basic chronology statistics and assessment. In: Cook, E.R., Kairiukstis, L. (Eds.), Applications in the Environmental Science. Kluwer, Dordrecht, pp. 137–152.

Case, R.A., MacDonald, G.M., 2003. Tree ring reconstructions of streamflow for three Canadian prairie rivers. Journal of American Water Resources Association 39, 703–716.

Cayan, D.R., Redmond, K.T., Riddle, L.G., 1999. ENSO and hydrologic extremes in the Western United States. Journal of Climate 12, 2881–2893.

Chao, Y., Ghil, M., McWilliams, J.C., 2000. Pacific interdecadal variability in this century's sea surface temperatures. Geophysical Research Letters 27, 2261–2264.

Collins, M., Osborn, T.J., Tett, S., Briffa, K.R., Schweingruber, F.H., 2002. A comparison of the variability of a climate model with paleotemperature estimates from a network of tree-ring densities. Journal of Climate 15, 1497–1515.

Cook, E.R., 1985. A Time Series Analysis Approach to Tree-ring Standardization. Ph.D. dissertation, University of Arizona, Tuscon.

Cook, E.R., 2000. El Nino 3 index reconstruction. In: International Tree-Ring Data Bank, IGBP PAGES/World Data Center-A for Paleoclimatology Data Contribution Series.

Cook, E.R., Kairiukstis, L.A. (Eds.), 1990. Methods of Dendrochronology, Applications in the Environmental Sciences. Kluwer Academic Publishers, Dordrecht, pp. 98–105.

Cook, E.R., D'Arrigo, R., Mann, M.E., 2002. A well-verified, multiproxy reconstruction of the winter North Atlantic Oscillation index since A.D. 1400. Journal of Climate 15, 1754–1764.

Cook, E.R., Woodhouse, C.A., Eakin, C.M., Meko, D.M., Stahle, D.W., 2004. Long-term aridity changes in the western United States. Science 306, 1015–1018.

Cook, E.R., Seager, R., Cane, M.A., Stahle, D.W., 2007. North American drought, reconstructions, causes, and consequences. Earth Science Reviews 81, 93–134.

Cook, E.R., D'Arrigo, R., Anchukaitis, K.J., 2008. ENSO reconstructions from long tree-ring chronologies, unifying the differences. In: Talk Presented at a Special Workshop on Reconciling ENSO Chronologies for the Past 500 Years, Held in Moorea, French Polynesia on 2–3 April 2008.

D'Arrigo, R., Wilson, R., 2006. On the Asian expression of the PDO. International Journal of Climatology 26, 1607–1617.

D'Arrigo, R., Villalba, R., Wiles, G., 2001. Tree-ring estimates of Pacific decadal climate variability. Climate Dynamics 18, 219–224.

Dawdy, D.R., Matalas, N.C., 1964. Statistical and probability analysis of hydrologic data, part III, Analysis of variance, covariance and time series. In: Te Chow, Ven (Ed.), Handbook of Applied Hydrology, a Compendium of Water-resources Technology. McGraw-Hill Book Company, New York, pp. 8.68–8.90.

Diaz, H.F., Hoerling, M.P., Eischeid, J.K., 2001. ENSO variability, teleconnections and climate change. International Journal of Climatology 21, 1845–1862.

Dracup, J.A., Lee, K.S., Paulson, E.G., 1980. On the statistical characteristics of drought events. Water Resources Research 16, 289–296.

Edwards, T.W.D., Birks, S.J., Luckman, B.H., MacDonald, G.M., 2008. Climatic and hydrologic variability during the past millennium in the eastern Rocky Mountains and northern Great Plains of western Canada. Quaternary Research 70, 188–197.

Fritts, H.C., 1976. Tree Rings and Climate. Academic Press, New York.

Fye, F.K., Stahle, D.W., Cook, E.R., 2003. Paleoclimatic analogs to twentieth-century moisture regimes across the United States. Bulletin of the American Meteorological Society 84, 901–909.

Gan, T.Y., Gobena, A.K., Wang, Q., 2007. Precipitation of southwestern Canada, wavelet, scaling, multifractal analysis, and teleconnection to climate anomalies. Journal of Geophysical Research 112. http://dx.doi.org/10.1029/2006JD007157.

Garnett, E.R., Nirupama, N., Haque, C.E., Murty, T.S., 2006. Correlates of Canadian Prairie summer rainfall, implications for crop yields. Climate Research 32, 25–33.

Gedalof, Z., Smith, D.J., 2001. Interdecadal climate variability and regime-scale shifts in Pacific North America. Geophysical Research Letters 28, 1515–1518.

Gedalof, Z., Mantua, N.J., Peterson, D.L., 2002. A multi-century perspective of variability in the Pacific Decadal Oscillation, new insights from tree rings and coral. Geophysical Research Letters 29, 57.1–57.4.

Gershunov, A., Barnett, T.P., 1998. Interdecadal modulation of ENSO teleconnections. Bulletin of the American Meteorological Society 79, 2715–2725.

Ghil, M., Allen, R.M., Dettinger, M.D., Ide, K., Kondrashov, D., Mann, M.E., Robertson, A., Saunders, A., Tian, Y., Varadi, F., Yiou, P., 2002. Advanced spectral methods for climatic time series. Review of Geophysics 40, 3.1–3.41.

Girardin, M.P., Sauchyn, D.J., 2008. Three centuries of annual area burned variability in northwestern North America inferred from tree rings. Holocene 18, 205–214.

Girardin, M.P., Tardif, J.C., Flannigan, M.D., Bergeron, Y., 2006. Synoptic-scale atmospheric circulation and boreal Canada summer drought variability of the past three centuries. Journal of Climate 19, 1922–1947.

Gray, S.T., Betancourt, J.L., Jackson, S.T., Eddy, R.G., 2006. Role of multidecadal climate variability in a range extension of pinyon pine. Ecology 87, 1124–1130.

Grinsted, A., Moore, J.C., Jevrejeva, S., 2004. Application of the cross wavelet transform and wavelet coherence to geophysical time series. Nonlinear Processes in Geophysics 11, 561–566.

Guttmann, N.B., 1998. Comparing the Palmer drought index and the standardized precipitation index. Journal of American Water Resources Association 34, 113–121.

Hamlet, A.F., Mote, P.W., Clark, M.P., Lettenmaier, D.P., 2007. Twentieth-century trends in runoff, evapotranspiration, and soil moisture in the Western United States. Journal of Climate 20, 1468–1486.
Herweijer, C., Seager, R., Cook, E.R., 2006. North American droughts of the mid to late nineteenth century, history, simulation and implications for Medieval drought. Holocene 16, 159–171.
Hughes, M.K., 2002. Dendrochronology in climatology – the state of the art. Dendrochronologia 20, 95–116.
Hurrell, J.W., Deser, C., 2009. North Atlantic climate variability, the role of the North Atlantic Oscillation. Journal of Marine Systems 78, 28–41.
IPCC4, 2007. In: Solomon, S., Qin, D., Manning, M., Chen, Z., Marquis, M., Avery, K.B., Tignor, M., Miller, H.L. (Eds.), Climate Change 2007, the Physical Science Basis. Contribution of Working Group I to the Fourth Assessment Report of the Intergovernmental Panel on Climate Change. Cambridge University Press, Cambridge, UK.
Kalnay, E., Kanamitsu, M., Kistler, R., Collins, W., Deaven, D., Gandin, L., Iredell, M., Saha, S., White, G., Woollen, J., Zhu, Y., Leetmaa, A., Reynolds, R., Chelliah, M., Ebisuzaki, W., Higgins, W., Janowiak, J., Mo, K.C., Ropelewski, C., Wang, J., Jenne, R., Joseph, D., 1996. The NCEP/NCAR 40-year reanalysis project. Bulletin of the American Meteorological Society 77, 437–471.
Kharin, V.V., Zwiers, F.W., Zhang, X., Hegerl, G.C., 2007. Changes in temperature and precipitation extremes in the IPCC ensemble of global coupled model simulations. Journal of Climate 20, 1419–1444.
Kiem, A.S., Verdon-Kidd, D.C., 2011. Steps towards 'useful' hydroclimatic scenarios for water resource management in the Murray-Darling Basin. Water Resources Research 47, W00G06. http://dx.doi.org/10.1029/2010WR009803.
Kiem, A.S., Franks, S.W., Kuczera, G., 2003. Multi-decadal variability of flood risk. Geophysical Research Letters 30, 1035. http://dx.doi.org/10.1029/2002GL015992.
Kim, K.W., North, G.R., 1993. EOF analysis of surface temperature field in a stochastic noise model. Journal of Climate 6, 1681–1690.
Keyantash, J., Dracup, J.A., 2002. The quantification of drought, an analysis of drought indices. Bulletin of the American Meteorological Society 83, 1167–1180.
Knox, J.L., Lawford, R.G., 1990. The relationship between Canadian Prairie dry and wet months and circulation anomalies in the mid-troposphere. Atmosphere-Ocean 28, 189–215.
Lapp, S.L., St. Jacques, J.M., Barrow, E.M., Sauchyn, D.J., 2012. GCM projections for the Pacific Decadal Oscillation under greenhouse forcing for the early 21st century. International Journal of Climatology 32, 1423–1442. http://dx.doi.org/10.1002/joc.2364.
Lau, N.C., 1997. Interactions between global SST anomalies and the midlatitude atmospheric circulation. Bulletin of the American Meteorological Society 78, 21–33.
Luckman, B.H., Wilson, R.J.S., 2005. Summer temperature in the Canadian Rockies during the last millennium, a revised record. Climate Dynamics 24, 131–144.
Lui, J., Stewart, R.E., Szeto, K.K., 2004. Moisture transport and other hydrometeorological features associated with the severe 2000/01 drought over the Western and Central Canadian prairies. Journal of Climate 17, 305–319.
MacDonald, G.M., Case, R.A., 2005. Variations in the Pacific Decadal Oscillation over the past millennium. Geophysical Research Letters 32. http://dx.doi.org/10.1029/2005GL022478.
Mann, M.E., Lees, J.M., 1996. Robust estimation of background noise and signal detection in climatic time series. Climatic Change 33, 409–445.
Mann, M.E., Bradley, R.S., Hughes, M.K., 2000. Multi-scale Variability and Global and Regional Impacts, Chap. Long-term Variability in the El Nino-Southern Oscillation and Associated Teleconnections. Cambridge University Press. 357–412.
Mantua, N.J., Hare, S.R., 2002. The Pacific Decadal Oscillation. Journal of Oceanography 58, 35–44.
Mantua, N.J., Hare, S.R., Zhang, Y., Wallace, J.M., Francis, R.C., 1997. A Pacific interdecadal climate oscillation with impacts on salmon production. Bulletin of the American Meteorological Society 78, 1069–1079.
Marchildon, G.P., Kulshreshtha, S., Wheaton, E., Sauchyn, D., 2008. Drought and institutional adaptation in the Great Plains of Alberta and Saskatchewan, 1914–1939. Natural Hazards 3, 391–411.
McGregor, S., Timmerman, A., Timm, O.A., 2010. Unified proxy for ENSO and PDO variability since 1650. Climate of the Past 6, 1–17.
McKenney, D.W., Pedlar, J.H., Papadopol, P., Hutchinson, M.F., 2006. The development of 1901-2000 historical monthly climate models for Canada and the United States. Agricultural and Forest Meteorology 138, 69–81.
Meko, D., Stockton, C.W., Boggess, W.R., 1995. The tree-ring record of severe sustained drought. Water Resources Bulletin 31, 789–801.
Meko, D.M., Woodhouse, C.A., Baisan, C.A., Knight, T., Lukas, J.J., Hughes, M.K., Salzer, M.W., 2007. Medieval drought in the Upper Colorado River Basin. Geophysical Research Letters 34. http://dx.doi.org/10.1029/2007GL029988.
Minobe, S., 1997. A 50–70 year climatic oscillation over the North Pacific and North America. Geophysical Research Letters 24, 683–686.
Minobe, S., 1999. Resonance in bidecadal and pentadecadal climate oscillations over the North Pacific, role in climatic regime shifts. Geophysical Research Letters 26. http://dx.doi.org/10.1029/1999GL900119.
Newton, A., Thunell, R., Stott, L., 2006. Climate and hydrographic variability in the Indo-Pacific warm pool during the last millenium. Geophysical Research Letters 33. http://dx.doi.org/10.1029/2006GL027234.
Nyenzi, B., Lefale, P.F., 2006. El Niño Southern Oscillation (ENSO) and global warming. Advances in Geosciences 6, 95–101.
Overland, J.E., Wang, M., 2007. Future climate of the North Pacific Ocean. EOS 88, 178–182.
Palmer, W.C., 1965. Meteorological Drought. Department of Commerce Weather Bureau, Washington, D.C. Research Paper No. 45, U.S.
Pederson, G.T., Gray, S.T., Woodhouse, C.A., Betancourt, J.L., Fagre, D.B., Littell, J.S., Watson, E., Luckman, B.H., Graumlich, L.J., 2011. The unusual nature of recent snowpack declines in the North American Cordillera. Science 333, 332–335.
Peterson, D.W., Peterson, D.L., 2001. Mountain hemlock growth responds to climatic variability at annual and decadal time scales. Ecology 82, 3330–3345.
Pham, S.V., Leavitt, P.R., McGowan, S., Wissel, B., Wassenaar, L.I., 2009. Spatial and temporal variability of prairie lake hydrology as revealed using stable isotopes of hydrogen and oxygen. Limnology and Oceanography 54, 101–118.
Pomeroy, J.W., de Boer, D., Martz, L.W., 2005. Hydrology and Water Resources of Saskatchewan. Centre for Hydrology Report #1, University of Saskatchewan. http://www.usask.ca/hydrology/reports/CHRpt01_Hydrology-Water-Resources-Sask_Feb05.pdf.
Pomeroy, J.W., de Boer, D., Martz, L.W., 2007. Hydrology and water resources. In: Thraves, B., Lewry, M.L., Dale, J.E., Schlichtmann, H. (Eds.), Saskatchewan: Geographic Perspectives. Canadian Plains Research Centre, Regina, pp. 63–80.
Rasmussen, E.M., Carpenter, T.H., 1982. Variations in tropical sea surface temperature and surface wind fields associated with the Southern Oscillation/El Niño. Monthly Weather Review 110, 354–384.
Redmond, K.T., Koch, R.W., 1991. Surface climate and streamflow variability in the western United States and their relationship to large-scale circulation indices. Water Resources Research 9, 2381–2399.
Renwick, J.A., Wallace, J.M., 1996. Relationships between North Pacific wintertime blocking, El Niño, and the PNA pattern. Monthly Weather Review 124, 2071–2076.
Sachs, J.P., Sachse, D., Smittenberg, R.H., Zhang, Z., Battisti, D.S., Golubic, S., 2009. Southward movement of the Pacific intertropical convergence zone AD 1400–1850. Nature Geoscience 2, 519–525.
Sauchyn, D.J., Beaudoin, A.B., 1998. Recent environmental change in the southwestern Canadian Plains. Canadian Geographer 42, 337–353.
Sauchyn, D.J., Skinner, W.R., 2001. A proxy PDSI record for the southwestern Canadian Plains. Canadian Water Resources Journal 26, 253–272.
Sauchyn, D.J., Stroich, J., Beriault, A., 2003. A paleoclimatic context for the drought of 1999-2001 in the northern Great Plains. Geographical Journal 169, 158–167.
Sauchyn, D., Vanstone, J., Perez-Valdivia, C., 2011. Modes and forcing of hydroclimatic variability in the upper North Saskatchewan River Basin since 1063. Canadian Water Resources Journal 36, 205–218.
Seager, R., 2007. The turn of the century drought across North America, global context, dynamics and past analogues. Journal of Climate 20, 5527–5552.
Shabbar, A., 2006. The impact of El Niño-Southern Oscillation on the Canadian climate. Advances in Geosciences 6, 149–153.
Shabbar, A., Bonsal, B., Khandekar, M.L., 1997. Canadian precipitation patterns associated with the Southern Oscillation. Journal of Climate 10, 3016–3027.
Speer, J., 2010. Fundamentals of Tree-ring Research. University of Arizona Press, Tuscon, Arizona, USA.
Stokes, M.A., Smiley, T.L., 1968. An Introduction to Tree-ring Dating. University Arizona Press, Tucson, Arizona, USA.
St. George, S., Nielsen, E., 2002. Hydroclimatic change in southern Manitoba since A.D. 1409 inferred from tree rings. Quaternary Research 58, 103–111.
St. George, S., Meko, D.M., Girardin, M.P., MacDonald, G.M., Nielsen, E., Pederson, G.T., Sauchyn, D.J., Tardif, J.C., Watson, E., 2009. The tree-ring record of drought on the Canadian Prairies. Journal of Climate 22, 689–710.
St. George, S., Meko, D.M., Cook, E.R., 2010. The seasonality of precipitation signals embedded within the North American Drought Atlas. Holocene 20. http://dx.doi.org/10.1177/0959683610365937.
St. Jacques, J.M., Sauchyn, D.J., Zhao, Y., 2010. Northern Rocky Mountain streamflow records, global warming trends, human impacts or natural variability? Geophysical Research Letters 37. http://dx.doi.org/10.1029/2009GL042045.
St. Jacques, J.M., Lapp, S.L., Zhao, Y., Barrow, E., Sauchyn, D.J., 2013. Twenty-first century northern Rocky Mountain river discharge scenarios under greenhouse forcing. Quaternary International 310, 34–46. http://dx.doi.org/10.1016/j.quaint.2012.06.023.
Sun, D.-Z., 2003. A possible effect of an increase in the warm-pool SST on the magnitude of El Niño warming. Journal of Climate 16, 185–205.
Thomson, D.J., 1982. Spectrum estimation and harmonic analysis. Proceedings IEEE 70, 1055–1096.
Trenberth, K.E., 1990. Recent observed interdecadal climate changes in the northern hemisphere. Bulletin of the American Meteorological Society 71, 988–993.
Trenberth, K.E., 1997. The definition of El Niño. Bulletin of the American Meteorological Society 78, 2771–2777.
Trenberth, K.E., Hurrell, J.W., 1994. Decadal atmosphere-ocean variations in the Pacific. Climate Dynamics 9, 303–319.
Trenberth, K.E., Stepaniak, D.P., 2001. Indices of El Niño evolution. Journal of Climate 14, 1697–1701.
Vanstone, J.R., Sauchyn, D.J., 2010. *Q. macrocarpa* annual, early- and late-wood widths as hydroclimatic proxies, southeastern Saskatchewan, Canada. IOP Conference Series, Earth and Environmental Science 9.
Verdon, D.C., Franks, S.W., 2006. Long-term behavior of ENSO, interactions with the PDO over the past 400 years inferred from paleoclimate records. Geophysical Research Letters 33. http://dx.doi.org/10.1029/2005GL025052.
Verdon-Kidd, D.C., Kiem, A.S., 2010. Quantifying drought risk in a nonstationary climate. Journal of Hydrometeorology 11, 1019–1031.

Wallace, J.M., Gutzler, D.S., 1981. Teleconnections in the geopotential height field during the Northern Hemisphere winter. Monthly Weather Review 109, 784–812.
Watson, E., Luckman, B.H., 2004. Tree-ring based reconstructions of precipitation for the southern Canadian Cordillera. Climatic Change 65, 209–241.
Watson, E., Luckman, B.H., 2005a. Spatial patterns of preinstrumental moisture variability in the southern Canadian Cordillera. Journal of Climate 18, 2847–2863.
Watson, E., Luckman, B.H., 2005b. An exploration of the controls of pre-instrumental streamflow using multiple tree-ring proxies. Dendrochronologia 22, 225–234.
Wheaton, E., Wittrock, V., Kulshreshtha, S., Koshida, G., Grant, C., Chipanshi, A., Bonsal, B.R., 2005. Lessons Learned from the Canadian Drought Years of 2001 and 2002, Synthesis Report, Agriculture and Agri-Food Canada, Saskatchewan Research Council Publication No. 11602-11646E03, Saskatoon, SK.
Wise, E.K., 2010. Spatiotemporal variability of the precipitation dipole transition zone in the western United States. Geophysical Research Letters 37. http://dx.doi.org/10.1029/2009GL042193.
Woodhouse, C.A., 1997. Winter climate and atmospheric circulation patterns in the Sonoran Desert region, USA. International Journal of Climatology 17, 859–873.
Woodhouse, C.A., Stahle, D.W., Villanueva Diaz, J., 2012. Rio Grande and Rio Conchos water supply variability over the past 500 years. Climate Research 51, 125–136.
Yu, B., Zwiers, F.W., 2007. The impact of combined ENSO and PDO on the PNA climate, a 1,000-year climate modeling study. Climate Dynamics 29, 837–851.
Zhang, Y., Wallace, J.M., Battisti, D.S., 1997. ENSO-like interdecadal variability, 1900–1993. Journal of Climate 10, 1004–1020.